Published in final edited form as:
Neuroimage. 2011 September 1; 58(1): 109–121. doi:10.1016/j.neuroimage.2011.05.087.

The generation and validation of white matter connectivity importance maps

Amy Kuceyeski[a,*], **Jun Maruta**[b], **Sumit N. Niogi**[c], **Jamshid Ghajar**[b,d], and **Ashish Raj**[a]

[a]Imaging Data Evaluation and Analytics Laboratory (IDEAL), Dept. of Radiology, Weill Cornell Medical College, 515 E. 71st St., New York, NY 10065, USA

[b]Brain Trauma Foundation, 7 World Trade Center, 34th Floor, 250 Greenwich St, New York, NY 10007, USA

[c]Department of Radiology, Weill Cornell Medical College, 1300 York Ave., New York, NY 10065, USA

[d]Department of Neurological Surgery, Weill Cornell Medical College, 1300 York Ave., New York, NY 10065, USA

Abstract

Both the size and location of injury in the brain influences the type and severity of cognitive or sensorimotor dysfunction. However, even with advances in MR imaging and analysis, the correspondence between lesion location and clinical deficit remains poorly understood. Here, structural and diffusion images from 14 healthy subjects are used to create spatially unbiased white matter connectivity importance maps that quantify the amount of disruption to the overall brain network that would be incurred if that region were compromised. Some regions in the white matter that were identified as highly important by such maps have been implicated in strategic infarct dementia and linked to various attention tasks in previous studies. Validation of the maps is performed by investigating the correlations of the importance maps' predicted cognitive deficits in a group of 15 traumatic brain injury patients with their cognitive test scores measuring attention and memory. While no correlation was found between amount of white matter injury and cognitive test scores, significant correlations ($r > 0.68$, $p < 0.006$) were found when including location information contained in the importance maps. These tools could be used by physicians to improve surgical planning, diagnosis, and assessment of disease severity in a variety of pathologies like multiple sclerosis, trauma, and stroke.

Keywords

white matter importance map; brain connectivity networks; graph theory; tractography; prediction of impairment; traumatic brain injury

[*]Imaging Data Evaluation and Analytics Laboratory (IDEAL), Dept. of Radiology, Weill Cornell Medical College, 515 E. 71st St. (S-125), New York, NY 10065, USA, Tel: (212) 746-1723, Fax: (212) 746-4189, amk2012@med.cornell.edu (Amy Kuceyeski), jmaruta@braintrauma.org (Jun Maruta), sun2003@nyp.org (Sumit N. Niogi), ghajar@braintrauma.org (Jamshid Ghajar), asr2004@med.cornell.edu (Ashish Raj) .

1. Introduction

Many brain pathologies, including stroke, multiple sclerosis and traumatic brain injury result in functional disability. The location and size of the affected area greatly influences the level and type of disability that the patient incurs. Current MRI-based diagnosis and assessment of brain injury is primarily qualitative, involving subjective interpretation of severity and prediction of impairment based on a physician's general anatomic and physiologic knowledge or previous patient-based experience. Even when augmented by 3D imaging tools that allow for objective measurement of lesion or tumor volume, the effect on brain function cannot be sufficiently characterized. This shortcoming arises because functional impairment is determined by both the extent and location of damage, and can be properly assessed only by also elucidating the structural connectivity of the affected gray matter region to the rest of the brain via its white matter fiber architecture.

There have been, however, numerous studies correlating total lesion load with severity and prognosis in various diseases, without considering the location of damage. In particular, one study showed a statistically significant although moderate correlation (r = 0.3–0.5) of lesion load in MS with EDSS scores of disability (Filippi et al., 1996), while another found slightly higher correlation by combining information from various MR modalities (Mainero et al., 2001). The correlations are modest most likely because the location of the lesions plays a large role in the patient's disability. In fact, several studies using lesion location in their analysis have shown higher correlation with severity of disability in MS (Charil et al., 2003; Wilson et al., 2003; Vellinga et al., 2009) and with stroke severity and functional recovery in stroke (Menezes et al., 2007; Nazzal et al., 2009). In Menezes et al. (2007), various selected brain structures were assigned a level of influence in stroke severity by two physicians. Using this map, a higher correlation (r = 0.79, p = 0.035) was found with the National Institutes of Health Stroke Scale (NIHSS) scores than the correlation calculated by using only lesion volume (r = 0.62). Another study in normal and TBI subjects showed that the FA of particular tracts correlates better with various measures in the Attention Network Test (Niogi et al., 2008b, 2010). Singh et al. (2010) discovered white matter ROIs with decreased FA in TBI patients and identified white matter tracts that appeared in equivalent ROIs in a series of normal patients. While these studies show some promise in the consideration of spatial location of damage, none of these has taken into account the location of the damaged tissue or tracts with respect to disruption in the overall brain connectivity network in a spatially unbiased manner.

1.1. Diffusion Imaging and Tractography

The structural brain network has recently become an area of wide interest due to the advances in diffusion imaging that can elucidate white matter structures (Assaf and Pasternak, 2008). DTI is a modality in MRI, introduced by Basser et al. (1994), that enables the localization and characterization of white matter fasciculi in the brain by assuming the direction and magnitude of water molecule diffusion in the brain occurs at a higher rate along white matter tracts than across them. Measurements are taken in numerous directions and tensor decomposition is used to extract the direction and magnitude of parallel and perpendicular diffusivity of water molecules (Basser et al., 1994; Basser, 1995). Summary statistics of the magnitude of diffusivities, such as the mean or the normalized standard deviation (fractional anisotropy-FA), provide interpretable values and a basis for visualization and construction of the white matter tracts (called tractography) (Basser and Pierpaoli, 1996, 1998; Pierpaoli and Basser, 1996).

Many tractography algorithms have been developed that use diffusion information to map the location and size of probable white matter tracts in the brain. Streamline tractography algorithms, for example FACT (Mori et al., 1999), begin at a user defined seed voxel and

take steps in the direction of fastest diffusion. Failure of these methods occurs within voxels that contain noise or have fibers that are crossing, “kissing”, diverging or merging. In an attempt to overcome this limitation, probabilistic methods (Zhang et al., 2009; Behrens et al., 2003; Friman et al., 2006) measure the probability of connection between regions rather than the actual reconstruction of the white matter pathways. One probabilistic method (Iturria-Medina et al., 2008) considers the probability of connection between two brain regions to be proportional to the most probable tract between any voxel in the respective regions. Once the representations of the white matter tracts are constructed, the connectivity of different regions in the brain can be represented by a graph and analyzed using existing methods in graph theory. In recent years, graphs and networks have been used to describe and analyze many different complex social, biological, and mathematical phenomena (Strogatz, 2001). These approaches have been used to investigate brain structure (Sporns et al., 2004), function (Achard et al., 2006), and a combination of the two (Bowman et al., 2009).

1.2. Graph Theory and Its Application to the Brain Network

A graph $G = (V, E)$ is defined by a set of vertices V that are linked pairwise by edges E (Gondran and Minoux, 1984). In a graph that represents brain connections, vertices correspond to gray matter regions and edges to measures of their connectivity via white matter tracts. Edges in a graph can be assigned a capacity or weight e_{ij} that gives the strength of connection between any two vertices i and j, while the distance d_{ij} between vertices i and j can be taken as the inverse of the edge weight, i.e. $d_{ij} = 1/e_{ij}$. A path p_{kl} from vertex k to l is defined to be a set of vertices such that from each vertex in the set, an edge exists to the next sequential vertex. Once all of the possible paths between vertices k and l are found, each path’s length, denoted $|p_{kl}|$, can be found by summing the distances between sequential vertices and subsequently the shortest path $\widehat{p}_{kl}$ can be identified.

Three graph metrics, defined below, are used in this paper to quantify a graph’s characteristics and make comparisons. These metrics are defined as:

- characteristic path length (*cpl*): average length of the shortest path between all pairs of vertices, i.e. $cpl = \sum_{k,l \in V, k \neq l} |\widehat{p}_{kl}| / \left(n^2 - n\right)$,
- efficiency (*eff*): average of the inverse of the shortest path length, i.e. $eff = \sum_{k,l \in V, k \neq l} |\widehat{p}_{kl}|^{-1} / \left(n^2 - n\right)$,
- spectral radius (*sr*): two norm of the graph matrix, i.e. $sr = \| A \|_2$,

where $A \in R^{m \times m}$ is the symmetric matrix representing the connectivity graph of m gray matter regions in the brain, whose element a_{ij} in the i^{th} column and the j^{th} row correspond to the weight of the edge between gray matter regions i and j in the connectivity graph ($a_{ij} = 0$ for $i = j$).

There have been a few recent studies that show promise in exploring changes in brain connectivity network metrics in certain disease states. Zalesky et al. (2011) showed a decrease in the efficiency measure of structural connectivity networks in schizophrenic patients compared to normal controls. The same study found significant correlations between network efficiency and intellectual performance in normal controls, but not in the patient population. Lo et al. (2010) showed an increase in path length and a decrease in efficiency in Alzheimer’s patients compared to normal age-matched controls. In addition, a third study (Wen et al., 2011) showed lower brain network efficiency measures correlated with increased age and decreased cognitive performance.

1.3. Paper Contribution

Thus far, analyses of brain network connectivity changes have depended on tractography performed on brains affected by a disease, injury, or aging. It is not known, however, if tractography methods that are highly sensitive to noise can yield physiologically meaningful connectivity information in abnormal brains. The method proposed in this paper circumvents this problem by assigning to a white matter region its relative importance to network connectivity as an indicator of the amount of damage incurred when that region is compromised.

A way to systematically and objectively quantify a white matter region's importance to overall brain connectivity has not yet been developed. Building on preliminary results (Kuceyeski and Raj, 2010), the current work uses diffusion data, structural MR images of the brain, and graph theory to systematically assign importance with respect to overall brain connectivity to white matter regions to further elucidate the correspondence between lesion location and cognitive deficit. This information, presented in the form of a three dimensional quantitative connectivity importance map of the brain, can improve surgical planning, diagnosis, and assessment of disease severity in a variety of pathologies such as multiple sclerosis, trauma, and stroke. The importance map itself is constructed independently of any pathological disease state, so evaluation of a patient's brain disruption requires a measure of the individual's white matter integrity. Since the severity of TBI has been shown to correspond to a decrease in FA (Rutgers et al., 2008; Niogi et al., 2008a), this measure is used to assess a TBI patient's white matter integrity. Validation is performed by measuring the correlation of the predicted overall brain connectivity disruption with test scores that rate disability and cognitive deficit in TBI. While the correlations of conventional measures such as amount of injury alone with these test scores were not found to be significant, the addition of the importance map information results in higher correlations that are significant.

2. Materials and methods

2.1. Data

The data used in this study were collected under a joint study between Weill Cornell Medical College and the Brain Trauma Foundation. It consists of 14 normal controls' (9 male and 5 female) and 15 traumatic brain injury patients' (10 male and 5 female) structural MR scans (T1 - FSPGR) and High Angular Resolution diffusion Images (HARDI). The mild TBI subjects were recruited through referrals from local concussion clinics. The conditions for inclusion were blunt, isolated TBI, post-traumatic amnesia, and a Glasgow Coma Scale (GCS) score of 13-15 at time of injury. The conditions for exclusion were pregnancy, a history of neurological or psychiatric diagnosis, seizure (prior to the injury), or drug or alcohol abuse. The ages of the normal controls and TBI patients were 23.1 ± 4.7 and 35.4 ± 10.5, respectively, and all of the subjects were right-handed. The scans were performed 20.2 ± 17.4 months from the time of injury and all patients had a GCS of 15.

The data were collected on a 3 Tesla GE Signa EXCITE scanner (GE Healthcare, Waukesha, WI, USA). HARDI data were acquired using 55 isotropically distributed diffusion-encoding directions at $b = 1000$ s/mm^2 and one at $b = 0$ s/mm^2, acquired at 72 1.8-mm thick interleaved slices with no gap between slices and 128 × 128 matrix size that was zero-filled during reconstruction to 256 × 256 with a field of view (FOV) of 230 mm. The structural scan was an axial 3D inversion recovery fast spoiled gradient recalled echo (FSPGR) T1 weighted images (TE = 1.5 ms,TR = 6.3 ms, TI = 400 ms, flip angle of 15) with 230 mm FOV and 156 1.0-mm contiguous partitions at a 256 × 256 matrix. In addition to image data, two tests of cognitive function that measure different components of attention and verbal working memory were scored for the same set of patients, namely, the Attention

Network Test (ANT) (Fan et al., 2002) and California Verbal Learning Test - Second Edition (CVLT-II, Pearson, San Antonio, TX, USA) (Jacobs and Donders, 2007; Niogi et al., 2008b). Detailed patient characteristics, including cognitive test scores, are listed in Table A.4 of Appendix A.

2.2. Extracting healthy whole brain connectivity networks

The connectivity weights between two gray matter regions in the brain can be measured in a variety of ways, e.g. probability of connection or the amount of white matter tissue connecting them. The Anatomical Connection Strength (ACS) metric used here (Iturria-Medina et al., 2007) represents potential information flow between gray matter regions which is assumed to be related to the amount of nervous fibers connecting them. Essentially, ACS is estimated by summing the weight of connection between two regions over all the surface voxels of both regions and is considered to be proportional to the cross-sectional area of the connecting fibers. White matter tracts can be constructed and their weights assigned in many different ways. The process used here, as first described in Iturria-Medina et al. (2007) and used in Kuceyeski and Raj (2010) and Ivkovich et al. (in press), is briefly outlined in the next two paragraphs and summarized by Figure 1.

Individual Brain Atlases Statistical Parametric Mapping (IBASPM) (Alemá-Gómez et al., 2005), Statistical Parametric Mapping (SPM5) (Friston et al., 2006), and Automatic Anatomical Labeling (AAL) software packages (Tzourio-Mazoyer et al., 2002) were used in Matlab R2009a (Natick, MA, The Mathworks Inc.). Individual T1 image volumes were co-registered to standardized Montreal Neurological Institute (MNI) space (Collins et al., 1998) and tissue probability maps constructed using SPM. Tissue masks were created by assigning each voxel to the tissue class (gray matter, white matter, cerebrospinal fluid) of highest probability. The gray matter mask was then parcellated into a standard 116-region atlas using IBASPM and AAL. The parcellated atlas and tissue masks were subsequently mapped back to the subject's native T1 space and re-sliced to the diffusion volume resolution. The orientation distribution function (ODF) of raw diffusion data was fully reconstructed using a spherical harmonic representation of q-ball imaging (spQBI) as found in Hess et al. (2006).

The surface voxels of the parcellated cortical and subcortical structures were used to seed the tractography algorithm in corresponding regions in the diffusion volume. The tractography algorithm was initiated 50 times per voxel, a number that was as large as possible without compromising computational efficiency. Proposed and validated in Iturria-Medina et al. (2005) and used in Sotero et al. (2007), the tractography algorithm implemented here incorporates tissue classification probability and ODF information in a Bayesian manner, similar to work found in Behrens et al. (2003),Friman et al. (2006), and Lu et al. (2006). A tract terminated when the algorithm reached the boundary of an image volume, the edge of a gray matter region, a voxel not in the gray or white matter masks, or when the angle between subsequent steps exceeded $\pi/3$. The above tractography was performed and the connectivity graph calculated for each normal subject.

2.3. Creating the Importance Maps

A measure of importance was assigned to voxels in the white matter importance map using the data from the normal subjects via the following process:

1. The center of a voxel identified to be in the white matter was selected as the center point for the region of interest r_i. This region corresponded to the site of a "hypothetical lesion."
2. The small spherical portion r_i of radius 1.5 times the size of the voxel (see Appendix B for an explanation of radius size selection) was defined and white

matter tracts that passed through that region were removed from the collection of tracts.

3. The modified connectivity graph $A_{r_i} \in R^{m \times m}$ ($m = 116$) was computed for the new set of white matter tracts and compared to the normal subject's original connectivity graph A using the three metrics outlined in Section 1.2. These metrics give information related to the change in connectivity when that region r_i is removed. This quantity was then recorded in the voxel corresponding to the region r_i in the importance map I.

4. Steps 1-3 were repeated until all the white matter regions r_i were lesioned, and the importance map completed.

The result of this process is a three dimensional volume of white matter tissue in the brain, where each small section of tissue is assigned its own measure of importance that is exactly the amount of connectivity change that occurs when it (and only it) is removed. Figure 2 summarizes this process for a particular white matter region of interest. In addition, a tract probability count (TPC) map was constructed by adding the probabilities of the tracts going through the same regions r_i for which the importance map values were calculated. The individual subjects' importance maps, TPC map, and white matter probability map (WMP) from SPM were coregistered to common MNI space by the process outlined in Appendix C.

Other graph summary metrics are available, but the ones selected here are widely used in various applications. Characteristic path length and efficiency are commonly used metrics in graph theory and brain network analysis (Zalesky et al., 2011; Lo et al., 2010; Wen et al., 2011), and the spectral radius is a summary statistic of the graph. The methodology proposed here can be tailored for specific applications by choosing the most appropriate metric for the disease or the question being addressed.

2.3.1. Importance Map Scores per Subject

The FA maps of each TBI patient were calculated and coregistered to common MNI space applying the same procedure used on the importance maps, described in Appendix C, and then compared against the normal group by computing the z-scores per voxel. The Importance Weighted Severity Score (IWSS) given to each TBI patient is defined as

$$IWSS = (1/N) \sum_{i=1}^{N} z_i \times I_i,$$

where the value I_i is the importance map entry for voxel i and N the number of white matter voxels. Recall that there are three different importance maps, resulting in three different IWSSs per patient. Two other scores are also computed for each of the TBI patients: the Tract Probability Count Score (TPCS) and the White Matter Probability Score (WMPS) defined as

$$TPCS = (1/N) \sum_{i=1}^{N} z_i \times TPC_i \quad \text{and} \quad WMPS = (1/N) \sum_{i=1}^{N} z_i \times WMP_i,$$

respectively, where TPC_i and WMP_i are the tract probability count and white matter probability map values at voxel i. The entries in the importance, TPC and WMP maps were scaled so that their values were between 0 and 1 in order to ensure consistency of the different scores. The scores will be more negative if regions have lower FA (negative z-scores) and/or higher importance, tract count, or white matter probability. In addition, voxels

with an FA of less than 0.1 were excluded to ensure that only white matter structures were used. A list of the various image-derived scores per patient are given in Table A.3 of Appendix A.

3. Results and Discussion

3.1. Comparison of the Maps

Equivalent slices of the various normalized average importance maps, along with the average WMP map and average TPC map, are shown in Figure 3. The efficiency and spectral radius importance maps had only negative entries before scaling, signifying a loss in brain network efficiency and a decrease in the magnitude of the principle eigenvector of the network after hypothetical lesioning. This was an unsurprising fact, as it was expected that there would be some decrease in the network qualities if fibers are removed. Also expected was the increase in characteristic path length metric after lesioning, indicating an increase in distance between nodes in the brain network. The values in the importance maps appear quite different, which may mean that the measures provide complimentary information, i.e. disruption in one region may alter characteristic path length more than it does the spectral radius of the graphs. To investigate the maps' regional differences in a quantitative manner, the JHU-MNI-ss atlas, or so-called "Eve" atlas (Oishi et al., 2009), was used to parcellate the white matter into 106 regions and the average importance map score over the voxels in each region was calculated (for the list of regions and their rankings for each map, see Appendix D). Pearson's correlation of the white matter region scores among the different maps was calculated (Table 1). The efficiency map's correlation with the TPC map is highest at a value of $r = 0.74$, while the other two graph measures of path length and spectral radius also have a moderate correlation with efficiency ($r = 0.59$, $r = 0.53$). Visually the TPC and efficiency maps are similar, with less localization over the two hemispheres which indicates that these measures may be generally more robust. The WMP map correlations with the TPC map and the importance maps are moderate at best. The lowest correlation is between the spectral radius and the characteristic path length map, a result which can be seen visually as the two maps have highly localized regions of importance in opposite hemispheres.

3.2. White matter regions of high and low importance

The highest values in the TPC map appeared in superficial white matter, including frontal and occipital regions. In contrast, the importance maps generally had higher values in deep white matter structures. Probabilistic fiber tracking methods assign higher probabilities to shorter fibers and thus white matter that is close in proximity to the surface of gray matter regions may have a larger number of tracts with higher probability. This may mean that the TPC map is biased for larger values in the superficial white matter. It must be emphasized that this effect is not seen in the connectivity importance maps, as they consistently showed higher scores in the deep white matter structures. It seems that the graph theoretical measures used to compare intact and damaged brain networks were robust enough to overcome the potential limitations of probabilistic tractography (see the Limitations section 3.5 for more discussion of this issue).

In the efficiency map, the right cuneus white matter, left and right sagittal stratum, right posterior thalamic radiation and right lateral-frontal white matter had high importance. In contrast, the map created using the path length metric had high importance in many regions in the left hemisphere, including the anterior and posterior limbs of the left internal capsule and the left external capsule. For the spectral radius metric, right hemisphere regions dominated, including the right posterior thalamic radiation and right inferior occipital white matter. To find regions identified with high importance in the various maps, the regions

were assigned a rank of 1 to 106 depending on how important they were in the respective maps. These ranks were summed, and it was found that the right precuneus white matter, the right and left sagittal stratum, the right lingual white matter and the right posterior thalamic radiation were the most important across the connectivity map metrics. Also high on the list were the left and right hippocampal cingulum and the left and right inferior occipital white matter. The right precuneus white matter is a part of the resting network, and the sagittal stratum, as described in Schmahmann and Pandya (2006), is a major corticosubcortical white matter bundle that connects regions of the parietal, occipital, cingulate, and temporal regions to subcortical thalamic regions, the nuclei of the basis pontis, and other brainstem structures. For a complete list of rankings, see the table in Appendix D.

Regions with low values agreed among the three importance maps and TPC map. Those assigned low values were the column and body of the left fornix, the right fornix, the bilateral pontine crossing tracts, bilateral medial lemniscus, and bilateral cortico-spinal tracts. The inferior cerebellar peduncles and red nuclei also had low map values. These structures had less than 1% of the maximum tract probability count, which would explain the low values in the importance maps. This outcome may be an artifact, however, as the brainstem is susceptible to movement with cardiac pulsations during the scan, resulting in extremely noisy diffusion data, a low amount of reconstructed tracts, and therefore low connectivity importance in these regions. The low tract count does not necessarily mean these regions do not have fibers and are not important in the brain network, only that the non-pulse gated imaging method used here cannot adequately capture its fiber architecture.

3.3. Comparison to findings in the literature

Many of the regions implicated in the different effects measured by the ANT (Niogi et al., 2008b, 2010) were shown to be highly ranked in one or more of the importance maps. The left anterior corona radiata, listed in the top 15% of regions in the combined rank and in the path length map (Appendix D), was shown to have FA measures that correlated with the conflict effect of the ANT. The left and right splenium of the corpus callosum were found to be correlated with the orienting effect in the ANT; here those structures appeared in the top 35% of the efficiency importance map, with the right side of the structure appearing in the top 20% of the combined importance map rankings. The left posterior limb of the internal capsule, correlated to the alerting effect of the ANT, was third most important in the path length importance map while in contrast it was halfway down the lists of structures in the efficiency, spectral radius, and overall rank.

Other neurological studies have shown that strategic infarct dementia, a highly debilitating condition wherein the patient experiences fluctuating alertness, inattention, memory loss, apathy, abulia, and psychomotor retardation, results from stroke lesions in the genu of the internal capsule (Tatemichi et al., 1995). The importance map for path length that ranked the left anterior and posterior limbs of the internal capsule as the first and third most important white matter regions may be capturing a center of connectivity that is affected in this type of focal stroke.

3.4. Quantitative Validation of Maps

The hypothesis that the importance maps provide more information than just the amount or probability of white matter alone was tested by correlating the TBI patients' map scores with their tests of cognitive function. Smaller (more negative) IWSS scores for a patient indicate larger network disruption and/or greater FA loss, which should correspond to greater functional loss and more abnormal cognitive scores. Since the goal of the importance map is to capture overall brain network disruption, and is not function specific, the cognitive test score used to validate the map should be functionally unbiased. One solution is to create an

overall cognitive measure that combines the various tests of function (ANT and CVLT-II) into one score. The well-known process of Principal Component Analysis (PCA) (Pearson, 1901) was used to create a combined cognitive score that has maximal variance over the population and presumably captures all of the cognitive functions tested. The coefficients for each cognitive measure are given in the last column of Table 2; note that the coefficients are negative to mantain a positive correlation with the various imaging scores. Most of the weight is on the ANT mean, with a small contribution from the three other ANT scores. Due to the disparity in coefficients, future studies may focus only on correlations with the ANT mean score.

Table 2 lists Pearson's correlation of the average z scores of FA, the WMPS, the TPCS, and the three IWSS with each of the cognitive test scores and the combined cognitive measure found using PCA. Figure 4 shows the scatter plots and lines of best fit along with the root mean squared error (RMSE) of the fit. The correlations for the individual cognitive test scores are higher in general when including the WMP, TPC, and importance map information than the z-scores of FA alone. Only the correlations between the TPCS and IWSS scores and the ANT mean reaction time and the combined cognitive score are significant at a level of $\alpha = 0.05$ (with Bonferroni correction for multiple comparisons), with the efficiency IWSS being significant at an even higher level ($\alpha = 0.01$, with correction). The relatively low correlation that exists with the more specific cognitive measures like ANT alerting and conflict effects could be due to the lack of specificity of the map values to any functional subnetworks in the brain; recall that the maps measure overall brain connectivity disruption, which is better captured by the ANT overall mean reaction time or the combined cognitive measure.

It may be argued that graph theoretical measures for the TBI patients' brain network extracted from their own image data might provide more information about cognition loss than the importance map method. However, it is not known how well tracts can be reconstructed in brains with disease-induced structural changes, including TBI, but it is a research topic of much interest (Singh et al., 2010). As comparison, the connectivity matrices for each of the TBI patients were obtained using the same process for the normal subjects described in 2.2, and the graph metrics of efficiency and characteristic path length computed directly on them. The graph metrics were then checked for correlations with the same cognitive measures as listed in Table 2, but no correlations were found to be significant. Therefore, the IWSS scores that estimated connectivity changes in injured brains were a better predictor of cognitive performance than the properties of networks extracted using tractography on image data from the TBI patient population.

3.5. Limitations

Tractography is an imperfect tool at the present, especially in dealing with partial volume effects and crossing and kissing fibers. Probabilistic tractography, in particular, has drawbacks in that it assigns higher probabilities to shorter fibers and thus white matter that is adjacent to gray matter regions may have a larger number of tracts with higher probability. Therefore, it may be an artifact that the highest TPC values appeared in superficial WM regions. On the other hand, many U-fibers may be invisible to diffusion MRI due to limited spatial and angular resolution. The two effects may partially cancel each other, but it is currently impossible to quantify the extent of these effects. The advancement of tractography techniques should remove many, if not all, of these concerns. It must be noted that this paper is not proposing an alternative method for tractography, but merely its use for important clinical and exploratory analyses. The importance maps proposed here will continue to be useful as enhancements to tractography algorithms are made.

Despite possible issues with tractography, the currently proposed methodology captures physiologically relevant white matter importance patterns whose validity was demonstrated by using TBI patient data. In fact, it was shown in Vaessen et al. (2010) that graph theoretical measures like clustering coefficient, characteristic path length, and node degree in brain connectivity networks were more reproducible between inter-subject scans and imaging protocols even when brain region connectivity measures themselves had lower levels of reproducibility. Thus, the use of graph theoretical measures to assess changes in diseased brains, as outlined in this paper, may be robust to the aforementioned limitations to tractography.

Coregistering individual brains that have anatomical abnormalities to a common space is a well-known and difficult problem. Co-registration is particularly difficult when working with atrophied or resected brains, and this specific issue is not investigated in the proposed work. In the mild TBI patient population used in this study, structural changes are not large enough to cause significant misregistration errors. If this method were to be applied to a clinical cohort with severe morphological changes, there are tools available to minimize coregistration errors, including the new DARTEL registration tool in SPM. For example, it was shown in Pereira et al. (2010) that DARTEL combined with pre-processing steps of skull-stripping and bias correction resulted in good registration of atrophied brains in Alzheimer's disease, Semantic Dementia, and behavioral-variant Frontotemporal Dementia.

4. Conclusions

A spatially unbiased quantitative method of assigning importance to regions of white matter with respect to overall brain connectivity using structural and diffusion MR images, tractography information, and graph theory is presented and validated. The importance map approach has the benefit that it does not require tractography to be performed in diseased brains, a notoriously difficult problem, in order to assess abnormalities in connectivity due to injury or disease. Importance map or tract probability count information better predicts cognitive scores in a set of TBI patients than the amount of white matter injury or injury information combined with white matter probability alone. It was found that the efficiency map provided IWSSs that were slightly better correlated to the outcomes of cognitive tests and of higher significance than the IWSS using other measures or the TPCS. The different metrics used to produce the white matter importance maps may provide complimentary information; therefore, they may be used to quantify varying types of cognitive disability. The current work does not assign a particular dysfunction to a location, but provides a measure of disruption in overall brain network that may correspond to more diffuse effects in brain function.

Even though the methodology presented here does not incorporate particular functional domain information, the white matter regions found to be important in some of the maps can be linked to specific pathological states. Regions of the internal capsule that were found to be important to brain network path length have been implicated in the particular cognitive dysfunction of strategic infarct dementia. White matter tracts shown to correlate with measures in the ANT, including the splenium of the corpus callosum, the left posterior limb of the internal capsule, and the left anterior corona radiata, were found to be highly ranked in one or more of the importance maps. Since it can be argued that the task of attention relates to general cognitive performance, this provides evidence that the importance maps are indeed measuring some aspect of overall brain function.

4.1. Future Work

In an extension of the current method, a series of more specific connectivity maps will be constructed for certain brain functions, such as motor control, eye movement, speech, or

sensory processing. Functionally specific connectivity maps will be constructed by calculating the importance map only for a subset of gray matter regions that are known to be linked to a particular function. Such maps will be validated with stroke or multiple sclerosis (MS) patients that have focal lesions and exhibit that specific cognitive or physical disability.

The importance map acts as a voxel-based spatial coefficient map to obtain a scalar value representing cognitive impairment (IWSS), but there will be extensions to non-scalar measures of cognitive impairment that further incorporate spatial information. For example, the dot-product of average z-scores and average importance map values for the 106 white matter regions will be computed and regressed with the cognitive scores.

Because white matter tracts vary in location and density from one individual to another, a tool providing probability of connection will be constructed. A database of normal subject's tracts will be created and subsequently validated using stroke and MS patients that exhibit specific cognitive or physical dysfunction. The patient's region of injury will be identified and a list of connecting gray matter regions and functions known to be associated with those regions will be produced and checked for accuracy against their clinical deficits.

Acknowledgments

The data processing, analysis, importance map creation and validation were supported by the following National Institutes of Health grants: F32 EB012404-01, P41 RR023953-02, P41 RR023953-02S1 and R21 EB008138-02. The data were collected and maintained with support from the Department of Defense grants W81XWH-08-1-0646 and W81XWH-08-2-0177, and a James S. McDonnell Foundation grant for the Cognitive Neurobiological Research Consortium in Traumatic Brain Injury. Rachel Kolster and Ranjeeta Sarkar provided assistance with subject enrollment and cognitive testing.

Appendix A. Patient Information

Table A.3

The 15 TBI patients' various scores derived from the analysis of the images.

Patient ID	Average z-scores	WMPS	TCPS	IWSS Spec. Rad.	IWSS Path Leng.	IWSS Eff.
1	0.0753	0.0073	−0.0002	−0.0015	−0.0009	0.0012
2	−0.0001	−0.0476	0.0053	0.0007	0.0004	−0.0012
3	0.0686	−0.0075	0.0032	0.0003	0.0008	0.0033
4	−0.0817	−0.0743	−0.0199	−0.014	−0.0073	−0.0237
5	−0.0964	−0.0693	−0.0104	−0.0077	−0.0015	−0.0107
6	−0.205	−0.0947	−0.0105	−0.0061	−0.0016	−0.0149
7	−0.0881	−0.0311	−0.0069	−0.0023	−0.0009	−0.0031
8	−0.1323	−0.0718	−0.0082	−0.0051	−0.0022	−0.012
9	−0.1024	0.0026	−0.005	0.0012	−0.0006	−0.0017
10	−0.0506	−0.0577	−0.0017	−0.0009	−0.0009	−0.0052
11	−0.2345	−0.1218	−0.0245	−0.0156	−0.006	−0.0276
12	0.044	−0.0616	−0.0034	−0.0044	−0.0012	−0.009
13	−0.0756	−0.0419	−0.0123	−0.006	−0.003	−0.0117
14	−0.092	−0.0031	−0.0081	−0.0031	−0.002	−0.0049
15	−0.1106	−0.0779	−0.0215	−0.0109	−0.0082	−0.0242

Table A.4

The 15 TBI patients' characteristics and cognitive scores, including the combined cognitive score.

Patient ID	Sex	Age	GCS	Mo. from injury	CVLT			ANT				Com-bined
					1	2	3	mean	1	2	3	
1	F	35	15	12	7	−1.5	−0.5	639.32	−14.75	77.89	75.90	−645.44
2	F	25	15	7	10	−0.5	−1	666.16	32.05	80.64	76.32	−673.83
3	M	45	15	51	11	0.5	1	678.05	13.46	27.53	152.01	−693.37
4	M	17	15	6	8	−1.5	−1	769.75	37.43	52.38	59.81	−772.90
5	F	29	15	29	10	−0.5	0.5	670.95	0.31	2.24	151.97	−684.82
6	M	40	15	18	7	−1	0.5	759.69	78.48	21.84	307.62	−797.98
7	M	26	15	10	13	0.5	0	579.64	7.73	35.92	74.72	−585.39
8	M	44	15	40	2	−2.5	−3.5	934.39	30.80	−21.77	15.16	−925.96
9	M	37	15	20	14	1	1	646.06	33.97	71.80	49.13	−649.88
10	F	52	15	53	10	0	0.5	653.26	46.42	60.11	132.88	−668.69
11	M	37	15	10	5	−2	−1.5	920.26	10.47	73.90	145.69	−933.67
12	F	49	15	35	10	0	0	816.91	77.92	−3.08	136.55	−829.45
13	M	20	15	1	16	2.5	1	802.69	58.18	75.73	126.69	−816.66
14	M	43	15	6	4	−2.5	1	1005.45	−59.02	−71.57	19.07	−787.55
15	M	32	15	3	9	−1	1	772.23	68.47	57.77	137.10	−991.52

Appendix B. Varying the hypothetical lesion radius

As demonstration, two slices in the spectral radius importance map for one individual are shown in Figure B.5 after varying the hypothetical lesion radius to 0.5, 1.5, and 2 times the voxel size. It can be seen by comparing the figures that the effect of this parameter is a smoothing and amplifying one: the larger the radius, the smoother the importance map and the higher the values. The smoothness is much to be expected, as it essentially acts as a filter in the image. Also expectedly, as the radius is expanded, more tracts are removed and a larger difference in network characteristics and higher values in the importance map are recorded. The selection of a lesion size of 1.5 times the voxel size was one that balanced smoothness and signal amplification in the resulting maps.

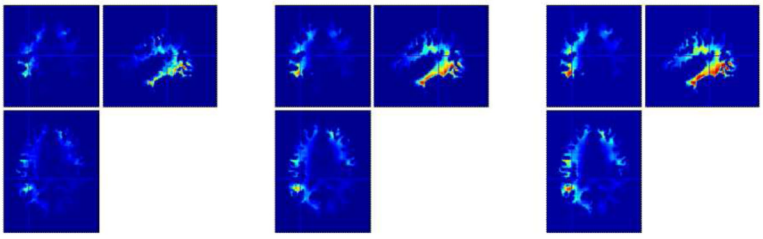

Figure B.5.

Appendix C. Co-registration of Individual Maps to a common space (MNI)

The importance, fractional anisotropy, white matter probability and tract probability count maps exist in the individual's native acquisition space, and in order to average across

subjects the maps must be transformed to a common template in MNI space using SPM's normalization routines. First, the T1 scans are mapped to the lower resolution diffusion image space using a 12-parameter a ne transformation, then the lower resolution T1 scan is normalized to a T1 MNI template in SPM by performing a 12-parameter a ne transformation followed by a non-linear warping transformation to estimate the 3D deformation field at each point. SPM uses a linear combination of 3D discrete cosine transform (DCT) basis functions in three orthogonal directions to model the deformation field. Once the parameters for transforming the low-resolution T1 image to MNI space were computed, and same transformation applied to the individual maps, checked visually for agreement and subsequently averaged, resulting in the final average map.

Appendix D. Importance Map Rankings of WM regions

Region Name	TC	IM Effic-iency	IM Path length	IM Spect. radius	Com-bined
cuneus wm right	11	1	6	12	1
sagittal stratum left	13	2	14	5	2
lingual wm right	44	7	11	10	3
sagittal stratum right	20	12	29	1	4
posterior thalamic radiation right	32	3	39	2	5
fusiform wm left	10	8	26	11	6
cingulum (hippocampus) left	6	13	17	27	7
inferior occipital wm left	5	11	45	7	8
superior longitudinal fasciculus right	28	6	35	23	9
posterior thalamic radiation left	51	15	38	13	10
cingulum (hippocampus) right	17	21	21	25	11
inferior occipital wm right	4	16	58	3	12
superior parietal wm left	21	4	40	36	13
anterior corona radiata left	15	29	12	40	14
middle occipital wm right	12	17	57	9	15
lateral fronto-orbital wm right	3	5	9	70	16
cingulum wm left	35	14	30	48	17
inferior frontal wm left	25	26	28	39	18
splenium of corpus callosum right	62	25	33	37	19
lingual wm left	40	33	42	21	20
inferior frontal wm right	14	9	31	57	21
middle fronto-orbital wm right	1	10	7	80	22
external capsule left	82	18	2	77	23
superior occipital wm right	8	19	62	17	24
lateral fronto-orbital wm left	7	20	16	62	25
fornix(cres) stria terminalis right	42	49	15	38	26
retrolenticular part of internal capsule left	73	47	8	52	27
supramarginal wm right	26	23	54	31	28
superior longitudinal fasciculus left	53	30	48	30	29
inferior temporal wm right	36	45	59	6	30

Region Name	TC	IM Effic-iency	IM Path length	IM Spect. radius	Com-bined
fornix(cres) stria terminalis left	76	50	5	58	31
fusiform wm right	23	46	60	8	32
middle fronto-orbital wm left	2	22	23	69	33
superior frontal wm right	27	24	49	43	34
superior parietal wm right	34	27	56	35	35
middle occipital wm left	19	39	65	16	36
cingulum wm right	49	32	46	44	37
precentral wm left	31	41	52	29	38
middle temporal wm right	55	48	71	4	39
superior frontal wm left	18	40	63	20	40
external capsule right	59	28	22	76	41
posterior limb of internal capsule right	64	42	13	72	42
splenium of corpus callosum left	61	35	44	49	43
anterior limb of internal capsule left	67	44	1	85	44
superior occipital wm left	9	36	68	26	45
precentral wm right	29	34	55	42	46
postcentral wm right	38	31	53	47	47
posterior limb of internal capsule left	83	51	3	79	48
anterior corona radiata right	30	37	32	66	49
retrolenticular part of internal capsule right	72	63	43	32	50
cerebral peduncle right	71	62	20	61	51
superior corona radiata left	68	60	51	33	52
inferior temporal wm left	52	57	74	14	53
supramarginal wm left	33	38	64	45	54
anterior limb of internal capsule right	65	43	19	87	55
cerebellum wm right	24	69	24	60	56
superior fronto-occipital fasciculus right	69	52	37	68	57
angular wm right	22	54	86	19	58
superior temporal wm right	58	70	79	15	59
superior temporal wm left	54	64	67	34	60
superior corona radiata right	63	56	61	50	61
middle frontal wm left	47	61	82	24	62
cerebral peduncle left	88	77	10	81	63
superior fronto-occipital fasciculus left	70	74	36	59	64
postcentral wm left	57	53	66	51	65
inferior fronto-occipital fasciculus left	46	68	18	86	66
substancia nigra left	92	78	4	90	67
middle cerebellar peduncle right	77	79	34	63	68
pre-cuneus wm right	60	55	69	53	69
posterior corona radiata left	80	59	72	46	70
posterior corona radiata right	79	71	80	28	71

Region Name	TC	IM Effic-iency	IM Path length	IM Spect. radius	Com-bined
middle temporal wm left	75	72	85	22	72
middle cerebellar peduncle left	81	84	27	75	73
tapatum right	85	80	90	18	74
pre-cuneus wm left	66	58	73	64	75
cuneus wm left	37	73	84	41	76
cingulum (cingulate gyrus) left	74	65	70	65	77
cerebellum wm left	45	83	47	74	78
substancia nigra right	90	82	41	82	79
middle frontal wm right	41	67	83	55	80
angular wm left	43	66	88	54	81
superior cerebellar peduncle right	91	91	25	93	82
inferior fronto-occipital fasciculus right	50	75	50	88	83
cingulum (cingulate gyrus) right	78	76	76	71	84
tapatum left	86	86	91	56	85
genu of corpus callosum left	48	87	75	73	86
rectus wm left	16	81	78	83	87
body of corpus callosum left	84	88	89	67	88
rectus wm right	39	85	77	91	89
genu of corpus callosum right	56	89	81	84	90
body of corpus callosum right	89	90	93	78	91
superior cerebellar peduncle left	93	93	87	97	92
uncinate fasciculus left	87	92	97	89	93
inferior cerebellar peduncle right	95	94	96	92	94
red nucleus left	100	95	92	98	95
red nucleus right	97	96	98	94	96
inferior cerebellar peduncle left	96	97	95	99	97
uncinate fasciculus right	94	98	99	95	98
medial lemniscus right	98	99	94	102	99
corticospinal tract right	101	102	103	96	100
corticospinal tract left	102	100	101	100	101
medial lemniscus left	99	101	100	103	102
pontine crossing tract right	105	104	102	101	103
pontine crossing tract left	103	103	104	104	104
fornix right	106	105	106	105	105
fornix (column and body) left	104	106	105	106	106

References

Achard S, Salvador R, Whitcher B, Suckling J, Bullmore E. A resilient, low-frequency, small-world human brain functional network with highly connected association cortical hubs. The journal of neuroscience. 2006; 26:63–72. http://www.ncbi.nlm.nih.gov/pubmed/16399673. [PubMed: 16399673]

Alemán-Gómez, Y.; Melié-García, L.; Valdés-Hernández, P. Ibaspm: Toolbox for automatic parcellation of brain structures; Presented at the 12th Annual Meeting of the Organization for Human Brain Mapping; Florence, Italy. 2005; http://www.thomaskoenig.ch/Lester/ibaspm.htm

Assaf Y, Pasternak O. Diffusion tensor imaging (dti)-based white matter mapping in brain research: a review. Journal of molecular neuroscience: MN. 2008; 24:51–61. http://www.ncbi.nlm.nih.gov/pubmed/18157658. [PubMed: 18157658]

Basser P. Inferring microstructural features and the physiological state of tissues from diffusion-weighted images. NMR in Biomedicine. 1995; 8:333–344. http://doi.wiley.com/10.1002/nbm.1940080707. [PubMed: 8739270]

Basser P, Mattiello J, LeBihan D. Mr diffusion tensor spectroscopy and imaging. Biophysical Journal. 1994; 66:259–267. http://linkinghub.elsevier.com/retrieve/pii/S0006349594807751. [PubMed: 8130344]

Basser P, Pierpaoli C. Microstructural and physiological features of tissues elucidated by quantitative-diffusion-tensor mri. Journal of Magnetic Resonance, Series B. 1996; 111:209–219. http://linkinghub.elsevier.com/retrieve/pii/S1064186696900862. [PubMed: 8661285]

Basser P, Pierpaoli C. A simplified method to measure the diffusion tensor from seven mr images. Magnetic resonance in medicine. 1998; 39:928–34. http://www.ncbi.nlm.nih.gov/pubmed/9621916. [PubMed: 9621916]

Behrens T, Woolrich M, Jenkinson M, Johansen-Berg H, Nunes R, Clare S, Matthews P, Brady J, Smith S. Characterization and propagation of uncertainty in diffusion-weighted mr imaging. Magnetic Resonance in Medicine. 2003; 50:1077–1088. [PubMed: 14587019]

Bowman F, Derado G, Chen S, Organization for Human Brain Mapping 2009 Annual Meeting. Evaluating functional connectivity using fmri data with diffusion-based anatomical weighting. NeuroImage. 2009; 47:S147–S147.

Charil A, Zijdenbos A, Taylor J, Boelmana C, Worsleya K, Evansa A, Dagher A. Statistical mapping analysis of lesion location and neurological disability in multiple sclerosis: application to 452 patient data sets. NeuroImage. 2003; 19:532–544. http://linkinghub.elsevier.com/retrieve/pii/S1053811903001174. [PubMed: 12880785]

Collins D, Zijdenbos A, Kollokian V, Sled J, Kabani N, Holmes C, Evans A. Design and construction of a realistic digital brain phantom. Medical Imaging, IEEE Transactions on 17. 1998:463–468.

Fan J, McCandliss BD, Sommer T, Raz A, Posner MI. Testing the efficiency and independence of attentional networks. Journal of Cognitive Neuroscience. 2002; 14:340–347. [PubMed: 11970796]

Filippi M, Mammi S, Martinelli V, Campi A, Colombo B, Scotti G, Canal N, Comi G. Correlation between brain mri lesion volume and disability in patients with multiple sclerosis. Acta Neurologica Scandinavica. 1996; 94:93–96. [PubMed: 8891052]

Friman O, Farneback G, Westin C. A bayesian approach for stochastic white matter tractography. IEEE Transactions on Medical Imaging. 2006; 25:965–978. [PubMed: 16894991]

Friston, K.; Ashburner, J.; Kiebel, S.; Nichols, T.; Penny, W. Statistical parametric mapping: The analysis of functional brain images. Academic Press; 2006. p. 656

Gondran, M.; Minoux, M. Graphs and Algorithms. John Wiley and Sons; 1984. Discreet Mathematics Series: 1-484

Hess C, Mukherjee P, Han E, Xu D, Vigneron D. Q-ball reconstruction of multimodal fiber orientations using the spherical harmonic basis. Magnetic Resonance in Medicine. 2006; 56:104–117. [PubMed: 16755539]

Iturria-Medina Y, Canales-Rodriguez E, Aleman-Gomez Y, Sotero R, Melie-Garcia L. Studying the human brain anatomical network via diffusion-weighted mri and graph theory. NeuroImage. 2008; 40:1064–76. http://www.ncbi.nlm.nih.gov/pubmed/18272400. [PubMed: 18272400]

Iturria-Medina, Y.; Canales-Rodriguez, E.; Melie-Garcia, L.; Valdes-Hernandez, P. Bayesian formulation for fiber tracking; Presented at the 11th Annual Meeting of the Organization for Human Brain Mapping; Toronto, Ontario, Canada. 2005; Available on CD-Rom in NeuroImage 26(1)

Iturria-Medina Y, Canales-Rodriguez E, Melie-Garcia L, Valdes-Hernandez P, Martinez-Montes E, Aleman-Gomez Y, Sanchez-Bornot J. Characterizing brain anatomical connections using diffusion weighted mri and graph theory. NeuroImage. 2007; 36:645–660. [PubMed: 17466539]

Ivkovich M, Kuceyeski A, Raj A. Statistics of weighted brain networks reveal hierarchical organization and gaussian degree distribution. PLOS One. in press.

Jacobs M, Donders J. Criterion validity of the california verbal learning test-second edition (cvlt-ii) after traumatic brain injury. Archives of clinical neuropsychology: the official journal of the National Academy of Neuropsychologists. 2007:143–149. http://www.ncbi.nlm.nih.gov/pubmed/17207963. [PubMed: 17207963]

Kuceyeski, A.; Raj, A. Analysis of connectivity of gray matter regions using dti and graph theory; Presented at the Joint Annual Meeting ISMRM-ESMRMB; Stickholm, Sweden. 2010; 2010. p. 1676

Lo C, Wang P, Chou K, Wang J, He Y, Lin C. Diffusion tensor tractography reveals abnormal topological organization in structural cortical networks in alzheimer?s disease. The Journal of Neuroscience. 2010; 30:16876–16885. [PubMed: 21159959]

Lu Y, Aldroubi A, Gore J, Anderson A, Ding Z. Improved fiber tractography with bayesian tensor regularization. NeuroImage. 2006; 31:1061–1074. [PubMed: 16563804]

Mainero C, DeStefano N, Iannucci G, Sormani M, Guidi L, Federico A, Bartolozzi M, Comi G, Filippi M. Correlates of ms disability assessed in vivo using aggregates of mr quantities. Neurology. 2001; 56:1331–4. http://www.ncbi.nlm.nih.gov/pubmed/11376183. [PubMed: 11376183]

Menezes NM, Ay H, Zhu MW, Lopez CJ, Singhal AB, Karonen JO, Aronen HJ, Liu Y, Nuutinen J, Koroshetz WJ, Sorensen AG. The real estate factor: quantifying the impact of infarct location on stroke severity. Stroke. 2007:194–197. http://stroke.ahajournals.org/cgi/content/full/38/1/194. [PubMed: 17122428]

Mori S, Crain B, Chacko V, Van Zijl P. Three-dimensional tracking of axonal projections in the brain by magnetic resonance imaging. Annals of Neurology. 1999; 45:265–269. http://doi.wiley.com/10.1002/1531-8249(199902)45:23.0.CO;2-3. [PubMed: 9989633]

Nazzal M, Saadah M, Saadah L, Trebinjac S. Acute ischemic stroke: relationship of brain lesion location and functional outcome. Disability and rehabilitation. 2009; 31:1501–6. http://www.ncbi.nlm.nih.gov/pubmed/19479508. [PubMed: 19479508]

Niogi S, Mukherjee P, Ghajar J, Johnson C, Kolster R, Sarkar R, Lee H, Meeker M, Zimmerman R, Manley G, McCandliss B. Extent of microstructural white matter injury in postconcussive syndrome correlates with impaired cognitive reaction time: a 3t diffusion tensor imaging study of mild traumatic brain injury. American Journal of Neuroradiology. 2008a; 29:967–73. [PubMed: 18272556]

Niogi S, Mukherjee P, Ghajar J, McCandliss B. Individual differences in distinct components of attention are linked to anatomical variations in distinct white matter tracts. Frontiers in Neuroranatomy. 2010; 4:1–12.

Niogi SN, Mukherjee P, Ghajar J, Johnson CE, Kolster R, Lee H, Suh M, Zimmerman RD, Manley GT, McCandliss BD. Structural dissociation of attentional control and memory in adults with and without mild traumatic brain injury. Brain. 2008b; 131:3209–3221. http://brain.oxfordjournals.org/cgi/reprint/131/12/3209.pdf. [PubMed: 18952679]

Oishi K, Faria A, Jiang H, Li X, Akhter K, Zhang J, Hsu J, Miller M, van Zijl P, Albert M, Lyketsos C, Woods R, Toga A, Pike G, Rosa-Neto P, Evans A, Mazziotta J, Mori S. Atlas-based whole brain white matter analysis using large deformation diffeomorphic metric mapping: Application to normal elderly and alzheimers' disease participants. Neuroimage. 2009:486–99. http://www.ncbi.nlm.nih.gov/pmc/articles/PMC2885858/. [PubMed: 19385016]

Pearson K. On lines and planes of closest fit to systems of points in space. Philosophical Magazine. 1901:559–572. http://stat.smmu.edu.cn/history/pearson1901.pdf.

Pereira J, Xiong L, Acosta-Cabronero J, Pengas G, Williams G, Nestora P. Registration accuracy for vbm studies varies according to region and degenerative disease grouping. NeuroImage. 2010; 49:2205–2215. [PubMed: 19892022]

Pierpaoli C, Basser P. Toward a quantitative assessment of diffusion anisotropy. Magnetic Resonance in Medicine. 1996; 36:893–906. http://doi.wiley.com/10.1002/mrm.1910360612. [PubMed: 8946355]

Rutgers D, Toulgoat F, Cazejust J, Fillard P, P. L, Ducreux D. White matter abnormalities in mild traumatic brain injury: a diffusion tensor imaging study. American journal of neuroradiology: AJNR. 2008; 29:514–9. http://www.ncbi.nlm.nih.gov/pubmed/18039754.

Schmahmann J, Pandya D. Fiber Pathways of the Brain. Oxford Scholarship Online Monographs. 2006

Singh M, Jeong J, Hwang D, Sungkarat W, Gruen P. Novel diffusion tensor imaging methodology to detect and quantify injured regions and affected brain pathways in traumatic brain injury. Magnetic Resonance Imaging. 2010; 28:22–40. [PubMed: 19608369]

Sotero R, Trujillo-Barreto N, Iturria-Medina Y, Carbonell F, Jimenez J. Realistically coupled neural mass models can generate eeg rhythms. Neural Computation. 2007; 19:478–512. http://www.mitpressjournals.org/doi/pdf/10.1162/neco.2007.19.2.478. [PubMed: 17206872]

Sporns O, Chialvo D, Kaiser M, Hilgetag C. Organization, development and function of complex brain networks. Trends in cognitive sciences. 2004; 8:418–25. http://www.ncbi.nlm.nih.gov/pubmed/15350243. [PubMed: 15350243]

Strogatz S. Exploring complex networks. Nature. 2001; 410:268–76. http://www.ncbi.nlm.nih.gov/pubmed/11258382. [PubMed: 11258382]

Tatemichi T, Desmond D, Prohovnik I. Strategic infarcts in vascular dementia: a clinical and brain imaging experience. Arzneimittel-Forschung. 1995; 45:371–385. http://cat.inist.fr/?aModele=afficheN&cpsidt=3479182. [PubMed: 7763329]

Tzourio-Mazoyer N, Landeau B, Papathanassiou D, Crivello F, Etard O, Delcroix N, Mazoyer B, Joliot M. Automated anatomical labeling of activations in spm using a macroscopic anatomical parcellation of the mni mri single-subject brain. NeuroImage. 2002; 15:273–289. [PubMed: 11771995]

Vaessen M, Hofman P, Tijssen H, Aldenkamp A, Jansen J, Backes W. The effect and reproducibility of different clinical dti gradient sets on small world brain connectivity measures. NeuroImage. 2010; 51:1106–1116. [PubMed: 20226864]

Vellinga M, Geurts J, Rostrup E, Uitdehaag B, Polman C, Barkhof F, Vrenken H. Clinical correlations of brain lesion distribution in multiple sclerosis. Journal of magnetic resonance imaging: JMRI. 2009; 29:768–73. http://www.ncbi.nlm.nih.gov/pubmed/19306365. [PubMed: 19306365]

Wen W, Zhu W, He Y, Kochan N, Reppermund S, Slavin M, Brodaty H, Crawford J, Xia A, Sachdev P. Discrete neuroanatomical networks are associated with specific cognitive abilities in old age. The Journal of Neuroscience. 2011; 31:1204–1212. [PubMed: 21273405]

Wilson M, Tench C, Morgan P, Blumhardt L. Pyramidal tract mapping by diffusion tensor magnetic resonance imaging in multiple sclerosis: improving correlations with disability. Journal of Neurology, Neurosurgery and Psychiatry. 2003; 74:203–207. http://jnnp.bmj.com/cgi/doi/10.1136/jnnp.74.2.203.

Zalesky A, Fornito A, Seal M, Cocchi L, Westin C, Bullmore E, Egan G, Pantelis C. Disrupted axonal fiber connectivity in schizophrenia. Biol Psychiatry. 2011; 69:80–9. [PubMed: 21035793]

Zhang F, Hancock E, Goodlett C, Gerig G. Probabilistic white matter fiber tracking using particle filtering and von mises-fisher sampling. Medical image analysis. 2009; 13:5–18. http://www.ncbi.nlm.nih.gov/pubmed/18602332. [PubMed: 18602332]

Highlights for Kuceyeski, et al.

- We create and validate a white matter connectivity importance map
- It gives the amount of connectivity disruption that occurs when a region is damaged
- Some tracts important in executive function were of high importance in maps
- We validate by correlating the map's prediction vs cognitive scores of TBI patients
- We find the correlation is higher when including map information

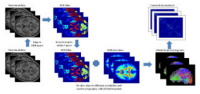

Figure 1.
The process by which the connectivity matrices or graphs are obtained.

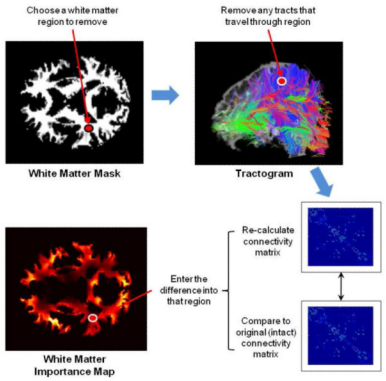

Figure 2.

The process by which the importance map is created. First, a region of white matter is identified and any tracts that pass through it are removed. The connectivity matrix is then re-computed and compared to the original intact matrix, and this difference is entered into the white matter region in the importance map. The difference is calculated in multiple ways, i.e. the difference in the spectral radii of the matrices, the difference in the graphs' efficiencies, and the difference in the graphs' path lengths.

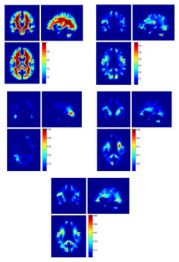

Figure 3.
The different maps in radiological coordinates (left of the image corresponds to the patient's right). (top-left) white matter probability, (top-right) tract probability count, (middle-left,middle-right,bottom) importance map using the difference in the spectral radius, characteristic path length and efficiency, respectively.

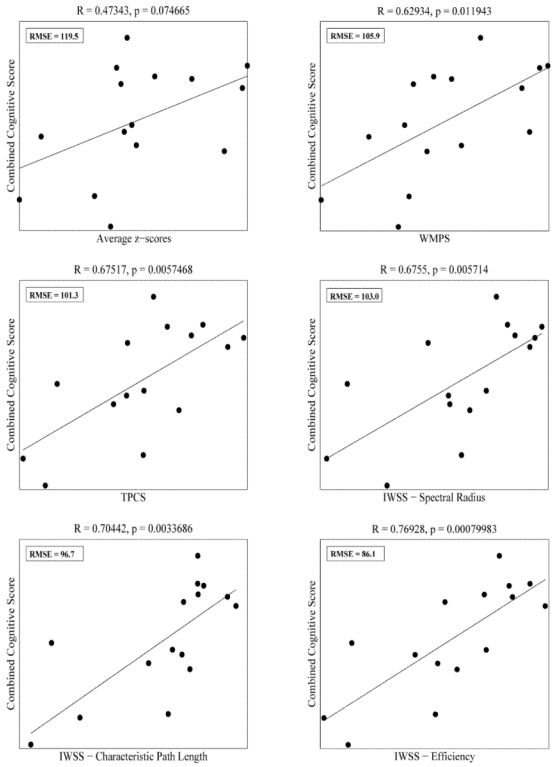

Figure 4.

Scatter plots of different scores (x-axis) versus the combined cognitive score (y-axis). The line of best fit and root mean squared error (RMSE) are also listed. The different scores are the average z-score of the FA (top left), the WMPS (top right), the TPCS (middle left), and the importance weighted severity score (IWSS) for three different metrics of network disruption: the difference in spectral radius (middle right), characteristic path length (bottom left), and efficiency (bottom right).

Table 1

Pearson's correlation of the average importance map value per white matter region and the WMP (white matter probability) map, the TPC (tract probability count) map, and the different importance maps (IM).

Map Metric	TPC	IM Spectral Radius	IM Path Length	IM Efficiency
WMP	0.21	0.04	0.28	0.21
TPC		0.36	0.33	0.74
IM Spectral Radius			0.05	0.53
IM Path Length				0.59

Table 2

Pearson's correlation of the average z-scores of FA, the WMPS, the TCPS, and the three IWSS with the various cognitive scores for the 15 TBI patients (CVLT - 1: long delay free recall, CVLT - 2: total recall discriminability, CVLT - 3: total recognition discriminability, ANT - 1: alerting, ANT - 2: orienting, ANT - 3: conflict), after Bonferroni correction for multiple comparisons. The correction is performed by dividing α by the number of candidate measures, which in this case is 6. The last column gives the coefficients used for that particular score in the combined (PCA) measure.

Cognitive Measure	Average z-scores	WMPS	TCPS	IWSS Spectral Radius	IWSS Path Length	IWSS Effic-iency	Com-bined Coeff.
CVLT - 1	0.31	0.52	0.37	0.48	0.46	0.51	−0.01
CVLT - 2	0.30	0.45	0.40	0.50	0.50	0.50	0
CVLT - 3	0.19	0.39	0.11	0.26	0.14	0.26	0
ANT - Mean	−0.45	−0.60	−0.67[a]	−0.67[a]	−0.72[a]	−0.76[b]	−0.99
ANT - 1	−0.06	0	0.23	0.21	0.36	0.15	−0.04
ANT - 2	0.12	0.35	0.28	0.27	0.33	0.34	−0.04
ANT - 3	−0.22	−0.25	0.04	−0.03	0.26	0.01	−0.14
Combined	0.47	0.63	0.68[a]	0.68[a]	0.70[a]	0.77[b]	

[a] significant at the level $\alpha = 0.05$

[b] significant at the level $\alpha = 0.01$